Sorption of paddy soil-derived dissolved organic matter on hydrous iron oxide-vermiculite mineral phases

Geoderma (2016) Volume 261, 169-177
doi: 10.1016/j.geoderma.2015.07.014

Sorption of paddy soil-derived dissolved organic matter on hydrous iron oxide-vermiculite mineral phases

Marcella Sodano[1,2], Daniel Said-Pullicino[*1,2], Antonio F. Fiori[1], Marcella Catoni[1], Maria Martin[1,2], Luisella Celi[1,2]

[1]*Soil Biogeochemistry, Dept. of Agricultural, Forest and Food Sciences, University of Torino, Grugliasco, Italy.*
[2]*Rice Agro-ecosystem and Environmental Research Group, Dept. of Agricultural, Forest and Food Sciences, University of Torino, Grugliasco, Italy.*

Abstract

Sorption of organic matter (OM) onto soil minerals affects OM dynamics, and is strongly controlled by mineral surface properties. Moreover, the degree and mechanism of interaction between different minerals may influence their surface reactivity. We therefore aimed to understand mineral surface modifications brought about by different Fe (hydr)oxide-vermiculite associations, and their influence on OM sorption. This could have important implications on OM dynamics in young hydromorphic soils where seasonal variations in redox conditions may affect mineral surfaces. Paddy soil-derived dissolved OM was used in sorption isotherms on mixed mineral phases obtained by precipitating different amounts of Fe (hydr)oxides on vermiculite. Results evidenced that the surface properties of vermiculite strongly drove Fe (hydr)oxide precipitation, and consequently OM sorption mechanisms. The change in surface charge with increasing Fe loading resulted in a higher retention of dissolved organic carbon. However, dissolved organic nitrogen adsorption isotherms and FTIR carboxyl vibrational shifts revealed the occurrence of two binding mechanisms, one driven by electrostatic attraction of N-containing compounds by the negatively charged vermiculite surface, and another involving ligand exchange of carboxylic compounds with the positive oxides, precipitated in localized nucleation sites. Moreover, the modification of both solution and solid properties during sorption, promoted the selective adsorption of aromatic molecules with increasing Fe coverage.

Keywords: Organic matter retention, clay mineralogy, surface properties, binding mechanisms, sorption isotherms.

[*] Corresponding Author
Daniel Said-Pullicino
Dept. of Agricultural, Forest and Food Sciences
University of Torino, Largo Paolo Braccini 2, 10095 Grugliasco, Italy.
E-mail: daniel.saidpullicino@unito.it

1. Introduction

The interaction of soil organic matter (OM) with the mineral phase is known to affect a variety of biogeochemical and environmental processes including the retention, preservation and accumulation of OM on one hand (Eusterhues et al., 2005; Kalbitz and Kaiser, 2008; Mikutta et al., 2007; Schneider et al., 2010; von Lützow et al., 2006), but also the rate of growth, degree of crystallization and consequently the surface reactivity of mineral phases on the other (Bachmann et al., 2008; Kaiser et al., 2007).

Organic matter sorption is primarily controlled by variable charge minerals, mainly iron (Fe) and aluminium (Al) (hydr)oxides (Feng et al., 2005; Kaiser et al., 1996; Wattel-Koekkoek et al., 2001). In particular, poorly crystalline (hydr)oxides can show a high retention capacity due to their large reactive surface area and positive charge at pH<8-9. However, in soil these oxides are often present, not as separated phases, but associated with or precipitated on other mineral particles, such as phyllosilicates. Association with metal (hydr)oxides modifies the properties of phyllosilicates, in particular electrical charge, specific surface area and porosity (Celi et al., 2003; Dimirkou et al., 1996). This results in complex mineral systems showing a different reactivity for OM which depends on the kind of phyllosilicate involved (Celis et al., 1998; Saidy et al., 2013), the percentage of Fe coverage (Celi et al., 2003), degree and mechanism of interaction (physical or chemical association) between the two minerals (Saidy et al., 2012; Sakurai et al., 1990), and chemical composition of the soil solution (Karim, 1984; Schwertmann and Thalmann, 1976).

Many studies have evaluated the effects of 1:1 phyllosilicate-Fe oxide associations (Arias et al., 1995; Celi et al., 2003; Celis et al., 1998; Dimirkou et al., 1996; Ioannou and Dimirkou, 1997; Jones and Saleh, 1986; Jones and Saleh, 1987; Sakurai et al., 1990; Yong and Ohtsubo, 1987), while less attention has been paid to 2:1 phyllosilicates. Saidy et al. (2012; 2013) showed that the capacity of illitic and smectitic clays to sorb dissolved organic matter (DOM)

was slightly affected by physical coating with different Fe oxides as a result of small variations in surface properties. This was in contrast with the findings of Celis et al. (1998) who reported that the surface area of montmorillonite-Fe oxide systems was much higher than that of the clay alone, and the pore structure depended on the amount of Fe in the system. To the best of our knowledge, no studies after Carstea et al. (1970) investigated vermiculite-Fe oxide systems. These phyllosilicates are particularly abundant in young hydromorphic soils (Cucu et al., 2014) where seasonal variations in redox conditions may induce the reductive dissolution and subsequent reprecipitation of Fe (hydr)oxides on 2:1 clays. In these soils, the frequent alternations in redox conditions may result in significant modification of mineral surfaces with important implications on the sorption and desorption of DOM. In fact, OM stabilization in hydromorphic soils, such as rice paddies, may be strongly controlled by sorption on Fe (hydr)oxide-vermiculite systems, particularly in temperate regions. We therefore hypothesized that (i) the precipitation of Fe (hydr)oxides on vermiculite may bring about important mineral surface modifications which depend on the amount of Fe loading, (ii) these changes may strongly influence the extent and mechanisms of OM sorption, and (iii) interaction between OM and mineral surfaces may modify the reaction environment, which, in turn, affects OM retention. To test these hypotheses we synthesized and characterized different hydrous Fe oxide-vermiculite mineral phases with increasing Fe loading, and evaluated their interaction with a paddy soil-derived DOM through sorption isotherms.

2. Materials and methods

2.1 Preparation and characterization of mineral phases

Vermiculite (VM), supplied by Palabora Mining Company (South Africa), was first milled and then purified. Briefly, carbonate salts were removed by treatment with sodium acetate

buffered at pH 4.8, Fe oxides by dithionite-citrate-bicarbonate, and OM by sodium hypochlorite oxidation at pH 8. The <1 μm fraction of purified VM was then separated by sedimentation, K-saturated with 1M KCl, washed with deionized water until salt-free, and freeze-dried. Small aliquots were was also Mg-saturated with 1M $MgCl_2$, and treated with ethylene glycol for spectroscopic analysis.

Four Fe (hydr)oxide-vermiculite systems (Fe-VM) with increasing proportions of Fe (1.3, 2.8, 4.7, and 5.6 mol Fe kg^{-1}, hereafter named 1Fe-VM, 2Fe-VM, 3Fe-VM and 4Fe-VM, respectively) were prepared by neutralizing different amounts of $Fe(NO_3)_3$ in a suspension of VM. For each system, 4 g of VM were dispersed in 800 mL of deionized water and left to equilibrate for 24 h under stirring. A known volume of 0.025 M $Fe(NO_3)_3$ at pH 2.0 was added dropwise to the VM suspension over 40 min under vigorous stirring. The pH of each suspension was then increased to 7.5 ± 0.3 with 1M KOH, and subsequently centrifuged, washed with deionized water until the electrical conductivity was <10 μS cm^{-1}, and freeze-dried.

The VM and the four *x*Fe-VM mixed systems were characterized for their mineralogical and surface properties. X-ray diffraction (XRD) spectra were acquired on air-dried oriented slides of the Mg- and K-saturated VM and mixed systems at 25 °C, and after thermal treatments at 105 and 300 °C (40kV and 20 mA, Fe filtered Co-Kα radiation; Philips PW 1710, Almelo, The Netherlands). Scans were made from 3 to 80º 2θ at a speed of 0.01º 2θ min^{-1}. The total content of precipitated Fe in the systems was determined by sodium dithionite-citrate-bicarbonate extraction (Fe_{DCB}; Mehra and Jackson, 1960), while the presence of poorly ordered Fe (hydr)oxides was estimated from the extraction of Fe with an ammonium oxalate solution buffered at pH 3.0 (Fe_O; Schwertmann, 1964). The specific surface area (SSA) and porosity of freeze-dried minerals were determined by adsorption-desorption of N_2 at 77 K after 24 h of out-gassing at 313 K under vacuum (<10^{-4} kPa) with a surface area analyzer

(Sorptomatic 1900, CarloErba, Rodano, Italy). The SSA was estimated by applying the Brunnauer-Emmet-Teller (BET) equation to the N_2 sorption data obtained in the relative pressure (p/p_0) range of 0.05 to 0.30 (Gregg and Singh, 1982). The SSA due to mesopores (2-50 nm) was derived from the adsorption branch of the isotherms using the Barrett-Joyner-Halenda model (Barrett et al.,1951), while the micropore surface (<2 nm) was calculated as the difference between the total SSA and the mesopore surface. The cation exchange capacity (CEC) was determined using the ammonium acetate method (Wilson, 1987), while the permanent negative charge (σ_0) was calculated as the ratio between the CEC and the SSA of each mineral. The zeta potential (ζ) was calculated from the electrophoretic mobility determined on a suspension adjusted to pH 5.5 and equilibrated for 24 h in 5 mM KCl, by Laser Doppler Velocimetry coupled with Photon Correlation Spectroscopy (LDV-PCS) using a spectrometer (DELSA 400, Beckman Coulter Inc., Hialeah, FL) equipped with a 5 mW He-Ne laser (632.8 nm).

2.2 Organic matter extraction and characterization

Water extractable organic matter (WEOM) and an alkali-extractable, acid-soluble OM fraction (AF) were obtained from a field fresh soil sampled from the Ap horizon (0-15 cm) of a rice paddy (Haplic Gleysol, NW Italy). These two OM pools were chosen to represent organic compounds stabilized on Fe (hydr)oxides under oxic conditions but potentially released into solution under anoxic conditions. Chemical and physical properties of the soil used were reported in Said-Pullicino et al. (2014). Briefly, WEOM was extracted from soil (<2 mm) with deionized water at a soil:solution ratio of 1:3 (w/v). After 2 h of shaking the suspension was centrifuged at 3500 rpm for 15 min, and the supernatant filtered through a 0.7-µm pore-sized glass fibre filter (GF/F, Whatman International Ltd., Maidstone, UK) and freeze-dried. The soil residue was subsequently extracted with 0.1 M NaOH using the same

soil:solution ratio for 16 h. The alkaline extract was then acidified to pH 1.0 allowing for the acid-insoluble fraction to precipitate, and subsequently the supernatant was filtered through 0.7-μm pore-sized glass fibre filter, purified on Amberlite XAD-8, protonated by passing through an Amberlite IR-120 strongly acidic cation exchange resin, and finally freeze-dried. Filtration of WEOM and AF extracts at 0.7 μm instead of the conventional 0.45 μm was adopted because OM released into solution under anoxic conditions could have a high charge to mass ratio and dimensions >0.45 μm. Different proportions of WEOM and AF fractions were mixed to obtain a single OM fraction having a C_{AF}/C_{WEOM} ratio of 2.22, similar to that determined in the bulk soil. Since this mixture was assumed to represent organic compounds potentially released into solution under reducing conditions, it will be hereafter called *r*DOM. The *r*DOM was characterized by chemical and spectroscopic analyses. Total C and N contents were determined by dry combustion (NA2500, Carlo Erba Instruments, Milano, Italy). Total acidity and carboxyl content were determined by potentiometric titration with $Ba(OH)_2$ and Ca acetate, respectively (Schnitzer and Gupta, 1965). Determination of the concentration of anions (Cl^-, NO_3^-, SO_4^{2-}, HPO_4^{2-}) was carried out by ion chromatography (AS50, Dionex, California; USA) while cations (K^+, Na^+, Mg^{2+}, Ca^{2+}, Fe^{3+}) were quantified by atomic absorption spectrometry (PerkinElmer AAnalyst 1400, USA). NH_4^+ concentration was determined spectrophotometrically by a modified Berthelot method involving reaction with salicylate in the presence of alkaline sodium dichloroisocyanurate (Crooke and Simpson, 1971). FTIR spectra of *r*DOM at pH 5.5 and 2.0 were acquired between 4000 and 400 cm^{-1} with a resolution of 4 cm^{-1} (PerkinElmer Spectrum 100, USA) on pellets obtained by pressing 1.0 mg of *r*DOM with 200 mg of KBr. Liquid-state ^{13}C NMR spectra were acquired with a 400 MHz spectrophotometer (Jeol EX-400, USA). An aliquot of 200 mg of freeze-dried material was dissolved in 1 ml of 0.5 M $NaOD/D_2O$. The spectra were recorded at a ^{13}C resonance frequency of 100.53 MHz with inverse-gated decoupling, 0.2 s acquisition time, a

45° pulse, and 2 s relaxation delay for a total acquisition time of 24 h. The free induction decays were processed by applying 50 Hz line broadening and baseline correction.

2.3 Sorption experiments

Sorption experiments were carried out in triplicate using *r*DOM solutions with concentrations ranging from 0 to 180 mg C l^{-1} prepared in 5 mM KCl and previously adjusted to pH 5.5. The different mineral phases (750 mg) were also dispersed in 5 mM KCl (250 mL), adjusted to pH 5.5 and shaken for 6 h at 25 °C. Then 5.0 mL of the suspensions containing 15 mg of each substrate, were added to 25 mL of the *r*DOM solutions and allowed to equilibrate for 16 h at 20 °C in the dark. The suspensions were then centrifuged, filtered at 0.7 µm (GF/F filters) and the equilibrium DOC concentration was determined by high-temperature combustion and infrared detection of CO_2 (Vario TOC, Elementar, Hanau, Germany). The amount of DOC sorbed onto the mineral phase (DOC_{ads} expressed in mg C g^{-1} or mg C m^{-2}) was calculated as the difference between initial and equilibrium DOC concentrations. Blank samples without sorbents were run for each experiment to assure that no mineralization or sorption to the containers had occurred. Sorption data were fitted into Langmuir (Eq. 1) and sigmoidal (Eq. 2) equations:

$$\mathrm{DOC}_{ads} = \frac{Q_{\max} \cdot K_L \cdot \mathrm{DOC}_e}{(1 + K_L \cdot \mathrm{DOC}_e)} \quad (1)$$

$$\mathrm{DOC}_{ads} = \frac{Q_{\max}}{1 + e^{-\left(\frac{\mathrm{DOC}_e - \mathrm{DOC}_{e0}}{b}\right)}} \quad (2)$$

where DOC_e is the equilibrium DOC concentration (mg C l^{-1}), Q_{max} is the maximum amount of sorbed DOC (mg C g^{-1} or mg C m^{-2}), and K_L is the Langmuir affinity constant (l mg^{-1}). In Eq. 2, DOC_{e0} is the equilibrium concentration corresponding to $Q_{max}/2$ at the inflection point and $1/b$ is the affinity constant calculated as the slope at the inflection point.

Selective adsorption of soluble N-containing compounds was evaluated by determining the initial and equilibrium dissolved organic nitrogen (DON) concentrations in the same *r*DOM solutions by elemental analysis (Vario TOC, Elementar, Hanau, Germany), and obtaining sorption data as described for DOC above. To evaluate the selective sorption of aromatic compounds, changes in the molar absorptivities of *r*DOM solutions before (ε_0) and after sorption (ε) were determined by measuring the UV absorbance at 254 nm (Helios, Thermo Electron, Massachusetts, USA) and normalizing for DOC concentrations (Weishaar et al., 2003). The pH of *r*DOM solutions before and after sorption was determined potentiometrically. Since Fe co-extracted with *r*DOM from the soil could influence DOC retention, Fe contents in the solutions before and after sorption were also determined by atomic absorption spectroscopy.

Changes in the electrophoretic mobility of the mineral phase after *r*DOM sorption were also determined on the suspensions at equilibrium after a 10-fold dilution with 5 mM KCl, by LDV-PCS as described above. Moreover, the chemical composition of sorbed *r*DOM was evaluated by FTIR. Mineral phases at the highest C loading were separated, washed with deionized water, dried and FTIR spectra were acquired as described above. Difference spectra [*r*DOM-(*x*Fe-VM) – (*x*Fe-VM)] were also obtained.

3. Results and Discussion

3.1 Properties of Fe (hydr)oxide-vermiculite systems

The results of XRD analyses on the phyllosilicate (VM) used in this work evidenced the presence of vermiculite and regular, mixed layer illite-vermiculite, identified by reflections at 1.43 nm, and 2.46 and 1.23 nm in the Mg-treated samples, respectively (Fig. 1a), and their collapse to 1.02 nm following K-saturation (Fig. 1b). The presence of smectites was excluded due the similarity in XRD patterns of samples treated with Mg and ethylene glycol (spectra

not shown). The introduction of Fe caused a shift in the 1.02 nm peak to higher *d*-spacing suggesting that some metal ions entered the interlayer (Fig. 1c-f). This shift, up to 1.21 nm, was more pronounced with increasing Fe contents, with the exception of the system with the highest Fe content (1.16 nm, 4Fe-VM, Fig. 1f). Heat treatment (105 °C) of the *x*Fe-VM systems always induced a collapse to 1.03-1.18 nm with the highest *d*-spacing obtained for 3Fe-VM (spectra not shown). Further heating to 300 °C did not cause any change in peak positions in the case of 1Fe-VM, while some further collapse (to 1.07-1.08 nm) was observed for 2Fe-VM and 3Fe-VM (spectra not shown). Hence, although some Fe could have entered the interlayer, this was probably only partial and showed a poor stability. On the other hand, the 4Fe-VM system showed a different behaviour. The shift of the first reflection from 1.02 to 1.16 nm was less pronounced suggesting that the presence of interlayered Fe was negligible in spite of the greater amount of Fe added with respect to the other Fe-VM systems. The scarce Fe-interlayering was in line with the limited effectiveness of Fe in forming interlayered phyllosilicates when added to montmorillonite or vermiculite (Carstea et al., 1970; Colombo and Violante, 1997). In fact, the narrow available space hinders the interlayering of vermiculite, favouring deposition of Fe (hydr)oxide at the edge margins (Carstea et al., 1970). With increasing amounts of added Fe, the intensity of the VM peaks decreased suggesting a strong association of the Fe (hydr)oxide with the negatively charged surfaces of the VM. The resulting aggregation could have also hampered the orientation of the VM crystals during sample drying leading to the broadening of reflection bands (Celis et al., 1998). Peaks at 0.46, 0.26, 0.24, 0.23, 0.22 and 0.15 nm, characteristic of six-line ferrihydrite (Eggleton and Fitzpatrick, 1988; Parfitt et al., 1992), were identified in the diffractograms of the mixed phases (Fig. 1c-f), the intensity of which increased slightly with increasing Fe content. Although distinctive peaks of crystalline Fe phases did not clearly appear, the formation of some micro-crystalline phases could however not be ruled out. In

fact, Violante and Huang (1994) reported that the detection of micro-crystalline oxides is substantially hampered in the presence of well crystallized phyllosilicates. With increasing Fe loading, the Fe_O/Fe_{DCB} ratio tended to increase slightly from 0.82 to 0.85 in the first three Fe-VM substrates, but decreased to 0.76 for 4Fe-VM (Table 1). This suggests that, apart from some crystallization, the lower oxalate extractability at highest Fe loadings could be attributed to particle aggregation promoted by the precipitation of Fe (hydr)oxides.

VM had a negative charge density of 15 $\mu mol_{(-)}\ m^{-2}$ and a ζ potential of –39 mV (pH 5.5). The precipitation of Fe (hydr)oxides on VM resulted in a decrease of negative charge density and an increase in the ζ potential (Table 1) that were correlated to the increasing Fe loading (r = –0.990 and 0.973, respectively). However, even at the highest Fe content (4Fe-VM) a negative charge was still preserved (5 $\mu mol_{(-)}\ m^{-2}$), and the measured ζ potential (+8 mV) was significantly lower than that generally reported for pure Fe (hydr)oxides (+40-50 mV; Kosmulski, 2014). These findings suggest that, even at highest Fe loading, the precipitated Fe (hydr)oxides did not completely coat the phyllosilicate surface (Celi et al., 2003), supporting the hypothesis of a non-homogeneous distribution of the (hydr)oxide on the VM surface.

The specific surface area (SSA) of VM, equally distributed between micro- and mesopores (Table 1), was particularly low when compared to natural vermiculites but nonetheless similar to other clay particles obtained by milling or sonication of the original silt-sized fraction (da Fonseca et al., 2006; Reinholdt et al., 2013). The SSA increased with increasing Fe loading, always with a similar distribution between micro- (45-52%) and mesopores (48-55%). However, at maximum Fe loading (4Fe-VM) mesopore surface dropped resulting in a consequent increase in the relative contribution of micropores to the total surface area (60%).

The increase in measured SSA was compared to the theoretical surface area ($SSA_{theoretical}$) calculated as the additive combination of the surface areas of each component:

$$SSA_{theoretical} = (1 - \theta)\cdot SSA_{VM} + \theta\cdot SSA_{Fh} \quad (3)$$

where SSA_{VM} and SSA_{Fh} are the measured SSA of vermiculite (20 m^2 g^{-1}) and ferrihydrite (150 m^2 g^{-1}) respectively, and θ is the proportion of ferrihydrite in each substrate (Table 1). Even considering the potential contribution of a more crystalline phase with a much lower SSA (Cornell and Schwertmann, 2003), the measured values strongly deviated from theoretical values particularly at the highest Fe loadings (Fig. 2), confirming that the (hydr)oxide did not precipitate as a separate phase. More likely poly[Fe(III)-OH] cations were attracted on negative cavities of VM by coulombic forces, promoting the localized clustering and precipitation of Fe (hydr)oxides in correspondence with the negative sites of VM (Carstea et al., 1970). This is in line with the progressive decrease in negative charge density and preservation of a negative charge even at the highest Fe concentrations. Moreover, the formation of a chemical Si–O–Fe bond at the edges of the phyllosilicate interspaces could have progressively blocked the access of Fe to the interlayers (Carstea et al., 1970), promoting aggregation in the mixed systems with a lower surface area than expected (Fig. 2).

3.2 Dissolved organic matter properties

The main characteristics of the paddy soil-derived DOM are summarized in Table 2. The *r*DOM showed a relatively high N content and hence a low C/N ratio. This was corroborated by the presence of a weak shoulder at 1575-1540 cm^{-1} in the FTIR spectrum at pH 2 (Fig. 3a) attributable to $R–NH_3^+$ and –CONH– stretching vibrations (Socrates, 2004). The peak at 1385 cm^{-1} could be due to NH_4^+ and NO_3^-, although these ions were present in low amounts (0.22 and 0.51 mmol g^{-1} C, respectively). These results suggest that, in contrast to DOM derived from other sources (Chorover and Amistadi, 2001; Kaiser 2003; Mikutta et al., 2007), the paddy-soil derived *r*DOM used in this work was rich in cationic N-containing groups. Moreover, *r*DOM showed a comparably low carboxylic acidity, while phenolic groups were

relatively abundant (*c.f.* Kaiser 2003; Kaiser and Guggenberger, 2007), probably due to the accumulation of lignin-derived constituents in paddy soils (Table 2). FTIR spectra at pH 2.0 and 5.5 (Fig. 3a and b) evidenced the presence of carboxyl groups with a shift in the –C=O asymmetric stretching band from 1720 to 1620 cm^{-1} following pH increase (Celi et al., 1997). The bands in the 1140-1000 cm^{-1} region, attributable to the –C–OH bending and –C–O stretching vibrations of hydroxyl groups, suggest the presence of an important saccharide component, as confirmed by the ^{13}C NMR spectrum in the 60-105 ppm region (Table 2). The ^{13}C NMR spectrum also evidenced a greater aliphatic than aromatic character. These results highlight the specific characteristics of *r*DOM obtained from the paddy soil. The major cations co-extracted with *r*DOM were K^+ (7.44 mmol g^{-1} C), Na^+ (4.63 mmol g^{-1} C) and Ca^{2+} (1.76 mmol g^{-1} C), while minor amounts of Fe^{3+} (0.21 mmol g^{-1} C) were also present. The major anions were Cl^- (8.76 mmol g^{-1} C) and SO_4^{2-} (5.03 mmol g^{-1} C).

3.3 Sorption of dissolved organic matter on minerals

The amount of DOC sorbed on VM was negligible for equilibrium DOC concentrations <52 mg C l^{-1} but increased with increasing DOC_e up to a maximum of 10 mg C g^{-1} (Fig. 4). DOC sorption was adequately described by the sigmoidal equation (Table 3). The presence of Fe (hydr)oxides enhanced the sorption of DOC with respect to VM, even at the lowest Fe loading (1Fe-VM; Fig. 4). In fact, DOC sorption onto this mineral phase, described by both Langmuir (R^2 = 0.87) and sigmoidal (R^2 = 0.89) models, reached a maximum sorption capacity (Q_{max}) of 25 and 18 mg C g^{-1}, respectively (Table 3). 2Fe-VM showed the highest sorption capacity (67 mg C g^{-1}) but this decreased drastically by 57-63 % with higher Fe loadings, such that 4Fe-VM had a maximum sorption capacity similar to that observed for 1Fe-VM. The Langmuir equation, that best described the interaction between DOC and the

three mineral phases with highest Fe loadings (2, 3 and 4Fe-VM), evidenced that the greatest affinity was observed for 3Fe-VM (K_L = 67 l g^{-1}) followed by 4Fe-VM (Table 3).

Selective adsorption of soluble N-containing compounds was evaluated through the isotherms of DON (Fig. 5). Among the mineral phases only VM and 1Fe-VM showed an interaction with DON over the experimental concentration range. In both these cases, the amount of DON adsorbed as a function of equilibrium DON followed a sigmoidal trend (Fig. 5). For the other Fe-VM systems no relationships were observed and the DON_{ads} values were lower than those obtained for VM and 1Fe-VM in most cases.

As expected, the limited sorption of DOC on VM was in line with the relatively low affinity of 2:1 phyllosilicates for OM with respect to poorly ordered oxides. Nonetheless, the maximum sorption capacity obtained was higher than that reported for vermiculite dispersed in 0.01M NaCl, and more similar to the values obtained in 0.01M $CaCl_2$ (Mikutta et al., 2007). Chorover and Amistadi (2001) also found comparable sorption capacities of forest floor DOC on montmorillonite. In both cases, the retention was modelled reasonably well using the Langmuir equation and explained by formation of Ca^{2+} bridging between DOM and the negatively charged phyllosilicates. In the present study, the good fit of DOC and DON sorption data with a sigmoidal model suggests that the interaction between *r*DOM and VM involved the selective retention of simple, positively charged, N-containing organic compounds on the negatively charged mineral surface by electrostatic forces (Chorover and Amistadi, 2001; Feng et al., 2005). This may be due to the higher amount of amino groups or oligopeptide residues present in the paddy soil-derived OM compared to that extracted from forest floors (Chorover and Amistadi, 2001; Kaiser, 2003; Mikutta et al., 2007). The limited adsorption at low equilibrium DOC and DON concentrations (<52 mg C l^{-1} and <4 mg N l^{-1} respectively), suggests that interaction between *r*DOM and VM only occurred when the concentration of positively charged organic N compounds was high enough to replace other

cations, such as K^+, from the exchange sites. Nevertheless, the retention of anionic organic compounds by a metal bridging cannot be excluded. In fact, comparison between equilibrium and initial concentrations of soluble Fe originally present within the *r*DOM solution (Fig. 6), suggested a slight retention of added Fe along with the adsorption of DOC onto vermiculite. This supported the hypothesis of the participation of DOC–Fe-VM metal bridging in the retention of *r*DOM.

The relative contribution of Fe (hydr)oxides to the retention of DOC on vermiculitic clay surfaces was evident even at the lowest Fe loading (i.e. 1Fe-VM). Although this mineral showed a strong retention of DOC at equilibrium concentrations <16 mg C l^{-1} probably due to the preferential sorption of DOC onto the Fe (hydr)oxide surfaces (Fig. 4), the presence of negative sites on the phyllosilicate surface with a charge density of 13 $\mu mol_{(-)}$ m^{-2} (Table 1) accounted for the sigmoidal trend at higher DOC_e, indicating that DOC binding mechanism was still driven by VM. This was probably further enhanced by the unstable Fe-VM phase. In fact, 1Fe-VM experienced the largest release of Fe into the solution with increasing DOC sorption (Fig. 6), suggesting that Fe may have been detached from the mineral phase as a consequence of the repulsion between the new negative surfaces determined by *r*DOM sorption (see detailed data on surface charge below) and the residual negative charges of VM. This was in line with the increasing detachment of Fe nanoparticles with increase DOC sorption on ferrihydrite-kaolinite systems reported by Celi et al. (2003). Nevertheless, the amount of DOC retained by 1Fe-VM was almost twice that of VM. The two mechanisms of *r*DOM sorption to 1Fe-VM were confirmed by the FTIR spectra of *r*DOM at pH 5.5 before and after sorption (Fig. 7a and b). In fact, adsorption resulted in the appearance of a weak shoulder at 1548 cm^{-1} attributable to $–NH_3^+$ and –CONH– vibrations (Socrates, 2004), confirming the retention of N-containing organic compounds on VM sites by cation exchange. On the other hand, the shift of the vibrational band relative to –C=O asymmetric

stretch (1629 cm^{-1}) to a lower frequency (1580 cm^{-1}), suggested the involvement, albeit limited, of carboxylate groups in the adsorption by ligand exchange through the formation of COO–Fe bonds (Gu et al., 1994).

The important increase in DOC sorption with increasing Fe loading was primarily related to the greater contribution of Fe (hydr)oxide to the specific surface area, although normalization of DOC sorption to the surface area gave a higher maximum coverage for 2Fe-VM (1.9 mg C m^{-2}) with respect to 1Fe-VM (1.1 mg C m^{-2}; Table 3). This was due to the fact that increasing the contents of Fe (hydr)oxide from 10.3 to 22.6 % not only increased the surface available for ligand exchange, but also contributed to reduce the negative charge of VM by half and shift the ζ potential from –39 to –10 mV (Table 1), favouring the attraction of negatively charged functional groups of *r*DOM towards the newly formed positive sites. This is consistent with the increase in intensity of the $–COO^-$ asymmetric stretching band and emergence of the $–COO^-$ symmetric stretch at 1580 and 1410 cm^{-1}, respectively (Fig. 7b and c), as observed for the sorption of DOC on pure Fe oxides (Gu et al., 1994; Kaiser and Guggenberger, 2007). These results indicate that the prevailing binding mechanism in the 2Fe-VM system involved ligand exchange on the (hydr)oxide surface with carboxyl groups. In contrast, the lack of a trend in the sorption of DON (Fig. 5) and the lack of a variation in solution Fe concentration (Fig. 6) with DOC sorption suggest that cation exchange and/or metal bridging on the phyllosilicate surface were negligible already at this Fe loading.

At even greater Fe loadings (3Fe-VM and 4Fe-VM) the affinity of the minerals for DOC increased drastically, although the maximum sorption capacity was less than half that obtained for 2Fe-VM (Table 3), and extremely low when compared to pure Fe oxides (Kaiser, 2003; Kaiser et al., 2007). At these Fe loadings, aggregation processes during the precipitation of Fe (hydr)oxides on the phyllosilicate surface and the proportional increase of micropores may limit the interaction of DOC exclusively to external surfaces (Buffle et al.,

1998; Kaiser and Guggenberger, 2007). This was confirmed by the lower maximum sorption capacity when normalized to initial surface area (0.65-0.74 mg C m^{-2}). Saidy et al. (2013) found that only the coating of illite with ferrihydrite rather than more crystalline iron oxides (goethite and hematite) increased the capability of illite to adsorb DOC. Therefore, the reduced retention capacity could be also attributed to the presence of more crystalline Fe (hydr)oxide phases in these systems. This was partially confirmed by the slightly lower Fe_O/Fe_{DCB} ratio obtained for 4Fe-VM with respect to the other mineral phases (Table 1). Ligand exchange governed the retention of DOC on the minerals with the greater Fe (hydr)oxide contents, as indicated by the sharper and more pronounced bands at 1580 and 1410 cm^{-1} (Fig. 7d and e), particularly evident in the 4Fe-VM system.

3.4 Sorptive fractionation of dissolved organic matter on minerals

The UV absorbance at 254 nm of *r*DOM normalized to DOC is an estimate for the aromaticity of OM (Weishaar et al., 2003) and has been used to evaluate changes upon contact of DOM with minerals (Chorover and Amistadi, 2001). Figure 8 shows the effect of sorption on the molar absorptivity of *r*DOM remaining in solution (ε) relative to the molar absorptivity of the initial *r*DOM solution (ε_0). For VM, $\varepsilon/\varepsilon_0$ remained relatively constant with increasing DOC_e concentrations, indicating that no selective sorption of aromatic compounds occurred with increasing DOC retention. Similar results were obtained by Mikutta et al. (2007) who reported a preferential sorption of aromatic OM on vermiculite only when Ca^{2+} was used as the background electrolyte. The presence of Fe (hydr)oxide coatings on VM induced a preferential retention of aromatic constituents, particularly at lower equilibrium DOC concentrations (Fig. 8). These findings imply that aromatic compounds interact selectively and strongly with the surface hydroxyl groups of the Fe (hydr)oxide, particularly at small DOC concentrations. This preferential sorption of aromatic OM increased with

increasing Fe loading in the order 1Fe-VM < 2Fe-VM < 3Fe-VM < 4Fe-VM, with $\varepsilon/\varepsilon_0$ values as low as 0.2 for the mineral phases with greatest (hydr)oxide coating. This could have been favoured by a greater micropore surface area (Table 1) and higher occupation of the micropores by the smaller aromatic components, as suggested by the good negative correlation between microporosity and $\varepsilon/\varepsilon_0$ values at the lowest equilibrium DOC concentration ($r = 0.954$, $p < 0.01$).

3.5 Effects of dissolved organic matter sorption on reaction environment

Sorption processes generally result in a modification of both mineral surface and solution properties. The sorption of *r*DOM on VM resulted in a small shift in initial pH values by about 0.5 units, reaching maximum equilibrium pH values of about 6.0 at lowest DOC_e concentrations (Fig. 9). This shift in initial pH tended to decrease with increasing equilibrium concentrations. In contrast, at DOC_e concentrations <52 mg C l^{-1} no changes in the ζ potential were observed with respect to the initial values, although the phyllosilicate surface became slightly less negative with increasing DOC_e reaching values of –31 mV at maximum sorption. The retention of positively charged N-containing functionalities on VM by exchange with protons and other cations may account for the lower solution pH as well as for the less negative ζ potential with increasing C loading.

Although the variation of solution pH with DOC sorption on 1Fe-VM showed a similar trend to VM, the retention of DOC on minerals with higher Fe loadings resulted in a strong increase in pH (from an initial pH of 5.5 to an equilibrium pH of 6.5-6.7) at DOC_e concentrations <8-13 mg C l^{-1}. Even here, equilibrium pH values tended towards initial values with increasing DOC_e concentrations. Ligand exchange involved in the interaction between carboxyl groups of *r*DOM and hydroxyl groups on the (hydr)oxide surface results in the release of OH^- in solution (Gu et al., 1994), leading to increasing pH values at low DOC_e

concentrations. At higher DOC concentrations the released OH^- may have been, however, partially consumed by the buffering capacity of the *r*DOM itself. This increase in solution pH values at low DOC_e concentrations was accompanied by a general decrease in the ζ potential of the Fe-VM minerals (Fig. 9) with respect to the initial values (Table 1). This decrease was most marked at highest Fe loadings, where the positive surface of 4Fe-VM (+8.0 mV) became immediately negative (–31 mV) following the sorption of even small amounts of *r*DOM (Tombácz et al., 2013), even though particle aggregation did not allow for the determination of ζ potentials at greater DOC_e concentrations (Fig. 9). Although the surface of Fe-VM systems was progressively less negative with increasing Fe loading, a lower amount of *r*DOM sorption was necessary to reach the most negative ζ potentials and the highest pH values.

While confirming that ligand exchange represented the dominant mechanism for *r*DOM sorption onto Fe-VM systems at higher Fe loadings, these results highlight the reciprocal influence that binding mechanisms and environmental factors of the soil solution have on each other. Alvarez-Puebla and Garrido (2005) showed how not only C loading, but also a variation in solution pH can have an important effect on self-assembling properties of heterogeneous organic molecules. The observed increase in pH to values around 6.7 due to DOC sorption on Fe (hydr)oxides, could promote the complete dissociation of carboxyl groups and also of phenolic functionalities having pK_a values of 5.9-7.0, particularly abundant in *r*DOM (Table 2). This could in turn influence the arrangement of sorbed molecules on the mineral surface and favour the preferential sorption of aromatic constituents, observed at low DOC concentrations, with the consequent displacement of molecules characterized by a lower affinity (Gu et al., 1996).

4. Conclusions

The presence of charged phyllosilicates like vermiculite in the clay-sized fraction of soils may strongly govern the precipitation of Fe. Our results have shown that vermiculite may promote the clustering and formation of non-homogeneous Fe (hydr)oxide coatings in correspondence with the negative sites of the phyllosilicate. In turn, the Fe loadings in these mixed mineral phases strongly affected charge density, pore distribution and particle aggregation. This may have important implications for the stabilization and accumulation of organic C, especially in soils subjected to alternating redox conditions. The redox-driven reductive dissolution and reprecipitation of Fe (hydr)oxides may result in the presence of reactive surfaces that range from “clean” phyllosilicates to highly coated hydrous iron oxide-phyllosilicate mixed systems. These different Fe loadings may not only affect the amount of sorbed organic matter, but also the binding mechanisms involved in the sorption process, and consequently the selective retention of particular constituents. Results showed that, whereas sorption of paddy soil-derived DOM on the vermiculite surface at low Fe loadings was controlled by cation exchange and involved interaction with N-containing organic compounds, increasing Fe (hydr)oxide contents enhanced sorption by ligand exchange with the selective retention of more aromatic compounds.

Acknowledgements

This study was part of the CarboPAD project (RBFR13BG31) funded by the Ministero dell' Istruzione, dell' Università e della Ricerca (MIUR) within the framework "Futuro in Ricerca 2013". Mike Darling of Palabora Europe Ltd. is acknowledged for supplying the vermiculite used in this work.

References

Alvarez-Puebla, R.A., Garrido, J.J., 2005. Effect of pH on the aggregation of a gray humic acid in colloidal and solid states. Chemosphere 59, 659-667.

Arias, M., Barral, M.T., Diaz-Fierros, F., 1995. Effects of iron and aluminium oxides on the colloidal and surface properties of kaolin. Clays & Clay Minerals 43, 406-416.

Bachmann, J., Guggenberger, G., Baumgartl, T., Ellerbrock, R.H., Urbanek, E., Goebel, M.-O., Kaiser, K., Horn, R., Fischer, W.R., 2008. Physical carbon-sequestration mechanisms under special consideration of soil wettability. Journal of Plant Nutrition and Soil Science 171, 14-26.

Barrett, E.P., Joyner, L.G., Halenda, P.H., 1951. The determination of pore volume and area distributions in porous substances. I. Computations from nitrogen isotherms. Journal of the American Chemical Society 73, 373-380.

Buffle, J., Wilkinson, K.J., Stoll, S., Filella, M., Zhang, J., 1998. A generalized description of aquatic colloidal interactions: The three-colloidal component approach. Environmental Science and Technology 32, 2887-2899.

Carstea, D.D., Harward, M.E., Knox, E.G., 1970. Comparison of iron and aluminium hydroxy interlayers in montmorillonite and vermiculite: I. Formation. Soil Science Society of America Proceedings 34, 517-521.

Celi, L., Schnitzer, M., Nègre, M., 1997. Analysis of carboxyl groups in soil humic acids by a wet chemical method, Fourier-transform infrared spectrophotometry, and solution-state carbon-13 nuclear magnetic resonance. A comparative study. Soil Science 162, 189-197.

Celi, L., De Luca, G., Barberis, E., 2003. Effects of interaction of organic and inorganic P with ferrihydrite and kaolinite-iron oxide systems on iron release. Soil Science 168, 479-488.

Celis, R., Cornejo, J., Hermosin, M.C., 1998. Textural properties of synthetic clay-ferrihydrite associations. Clay Minerals 33, 395-407.

Chorover, J., Amistadi, M.K., 2001. Reaction of forest floor organic matter at goethite, birnessite and smectite surfaces. Geochimica Cosmochima Acta 65, 95-109.

Colombo, C., Violante, A., 1997. Effect of ageing on the nature and interlayering of mixed hydroxy Al-Fe-montmorillonite complexes. Clay Minerals 32, 55-64.

Cornell, R.M., Schwertmann, U., 2003. The Iron Oxides: Structure, Properties, Reactions, Occurrences and Uses. Wiley-VCH Verlag GmbH & Co. KGaA, Weinheim.

Crooke, W.M., Simpson, W.E., 1971. Determination of ammonium in Kjeldahl digests of crops by an automated procedure. Journal of the Science of Food and Agriculture 22, 9-10.

Cucu, M.A., Said-Pullicino, D., Maurino, V., Bonifacio, E., Romani, M., Celi, L., 2014. Influence of redox conditions and rice straw incorporation on nitrogen availability in fertilized paddy soils. Biology and Fertility of Soils 50, 755-764.

da Fonseca, M.G., Cardoso, C.M., Wanderley, A.F., Arakaki, L.N.H., Airoldi, C., 2006. Synthesis of modified vermiculite by interaction with aromatic heterocyclic amines. Journal of Physics and Chemistry of Solids 67, 1835-1840.

Dimirkou, A., Ioannou, A., Kalliannou, C., 1996. Synthesis-identification of hematite and kaolinite hematite (k-h) system. Communications in Soil Science and Plant Analysis 27, 1091-1106.

Eggleton, R.A., Fitzpatrick, R.W., 1988. New data and a revised structural model for ferrihydrite. Clays and Clay Minerals 36, 111-124.

Eusterhues, K., Rumpel, C., Kögel-Knabner, I., 2005. Organo-mineral associations in sandy acid forest soils: Importance of specific surface area, iron oxides and micropores. European Journal of Soil Science 56, 753-763.

Feng, X., Simpson, A.J., Simpson, M.J., 2005. Chemical and mineralogical controls on humic acid sorption to clay mineral surfaces. Organic Geochemistry 36, 1553-1566.

Gu, B., Schmitt, J., Chen, Z., Liang, L., McCarthy, J.F., 1994. Adsorption and desorption of natural organic matter on iron oxide: Mechanisms and models. Environmental Science and Technology 28, 38-46.

Gu, B., Mehlhorn, T.L., Liang, L., McCarthy, J.F., 1996. Competitive adsorption, displacement, and transport of organic matter on iron oxide: II. Displacement and transport. Geochimica Cosmochima Acta 60, 2977-2992.

Gregg, S.J., Singh, K.S.W., 1982. Adsorption, surface area and porosity. Academic Press, London.

Ioannou, A., Dimirkou, A., 1997. Phosphate adsorption on hematite, kaolinite, and kaolinite-hematite (k-h) systems as described by a constant capacitance model. Journal of Colloid and Interface Science 192, 119-128.

Jones, A.A., Saleh, A.M., 1986. Electron diffraction and the study of ferrihydrite coatings on kaolinite. Clay Minerals 21, 85-92.

Jones, A.A., Saleh, A.M., 1987. A study of the thickness of ferrihydrite coatings on kaolinite. Mineralogical Magazine 51, 89-92.

Kaiser, K., Guggenberger, G., Zech, W., 1996. Sorption of DOM and DOM fractions to forest soils. Geoderma 74, 281-303.

Kaiser, K., 2003. Sorption of natural organic matter fractions to goethite (α-FeOOH): Effect of chemical composition as revealed by liquid-state ^{13}C NMR and wet-chemical analysis. Organic Geochemistry 34, 1569-1579.

Kaiser, K., Guggenberger, G., 2007. Sorptive stabilization of organic matter by microporous goethite: Sorption into small pores vs. surface complexation. European Journal of Soil Science 58, 45-59.

Kaiser, K., Mikutta, R., Guggenberger, G., 2007. Increased stability of organic matter sorbed to ferrihydrite and goethite on aging. Soil Science Societyof America Journal 71, 711-719.

Kalbitz, K., Kaiser, K., 2008. Contribution of dissolved organic matter to carbon storage in forest mineral soils. Journal of Plant Nutrition and Soil Science 171, 52-60.

Karim, Z., 1984. Characteristics of ferrihydrites formed by oxidation of $FeCl_2$ solutions containing different amounts of silica. Clays & Clay Minerals 32, 181-184.

Kosmulski, M., 2013. The pH dependent surface charging and points of zero charge. VI. Update. Journal of Colloid and Interface Science 426, 209-212.

Mehra, O.P., Jackson, M.L., 1960. Iron oxide removal from soils and clays by a dithionite-citrate system buffered with sodium bicarbonate. Clays & Clay Minerals 7, 317-327.

Mikutta, R., Mikutta, C., Kalbitz, K., Scheel, T., Kaiser, K., Jahn, R., 2007. Biodegradation of forest floor organic matter bound to minerals via different binding mechanisms. Geochimica Cosmochima Acta 71, 2569-2590.

Parfitt, R.L., Van Der Gaast, S.J., Childs, C.W., 1992. A structural model for natural siliceous ferrihydrite. Clays and Clay Minerals 40, 675-681.

Reinholdt, M.X., Hubert, F., Faurel, M., Tertre, E., Razafitianamaharavo, A., Francius, G., Prêt, D., Petit, S., Béré, E., Pelletier, M., Ferrage, E., 2013. Morphological properties of vermiculite particles in size-selected fractions obtained by sonication. Applied Clay Science 77-78, 18-32.

Said-Pullicino, D., Cucu, M.A., Sodano, M., Birk, J.J., Glaser, B., Celi, L., 2014. Nitrogen immobilization in paddy soils as affected by redox conditions and rice straw incorporation. Geoderma 228-229, 44-53.

Saidy, A.R., Smernik, R.J., Baldock, J.A., Kaiser, K., Sanderman, J., Macdonald, L.M., 2012. Effects of clay mineralogy and hydrous iron oxides on labile organic carbon stabilisation. Geoderma 173, 104-110.

Saidy, A.R., Smernik, R.J., Baldock, J.A., Kaiser, K., Sanderman, J., 2013. The sorption of organic carbon onto differing clay minerals in the presence and absence of hydrous iron oxide. Geoderma 209-210, 15-21.

Sakurai, K., Teshima, A., Kyuma, K., 1990. Changes in zero point of charge (ZPC), specific surface area (SSA), and cation exchange capacity (CEC) of kaolinite and montmorillonite, and strongly weathered soils caused by Fe and Al coatings. Soil Science and Plant Nutrition 36, 73-81.

Schneider, M.P.W., Scheel, T., Mikutta, R., van Hees. P,, Kaiser, K., Kalbitz, K., 2010. Sorptive stabilization of organic matter by amorphous Al hydroxide. Geochimica Cosmochima Acta 74, 1606-1619.

Schnitzer, M., Gupta, V.C., 1965. Determination of acidity in soil: organic matter. Soil Science of America Proceedings 29, 274-277.

Schwertmann, U., 1964. Differenzierung der Eisenoxide des Bodens durch Extraktion mit Ammoniumoxalat-Lösung. Zeitschrift für Pflanzenernährung, Düngung, Bodenkunde 105, 194-202.

Schwertmann, U., Thalmann, H., 1976. The influence of [Fe(II)], [Si], and pH on the formation of lepidocrocite and ferrihydrite during oxidation of aqueous $FeCl_2$ solutions. Clay Minerals 11, 189-200.

Socrates, G., 2004. Infrared and Raman Characteristic Group Frequencies: Tables and Charts. John Wiley & Sons Ltd., England.

Tombácz, E., Tóth, I.Y., Nesztor, D., Illés, A., Hajdú, A., Szekeres, M., Vékás, L. 2013. Adsorption of organic acids on magnetite nanoparticles, pH-dependent colloidal stability and salt tolerance. Colloids and Surfaces A 435, 91-96.

Violante, A., Huang, P.M., 1994. Identification of pseudoboehmite in mixtures with phyllosilicates. Clay Minerals 29, 351-359.

von Lützow, M., Kögel-Knabner, I., Ekschmitt, K., Matzner, E., Guggenberger, G., Marschner, B., Flessa, H., 2006. Stabilization of organic matter in temperate soils: mechanisms and their relevance under different soil conditions - a review. European Journal of Soil Science 57, 426-445.

Wattel-Koekkoek, E.J.W., Van Genuchten, P.P.L., Buurman, P., Van Lagen, B., 2001. Amount and composition of clay-associated soil organic matter in a range of kaolinitic and smectitic soils. Geoderma 99, 27-49.

Weishaar, J.L., Aiken, G.R., Bergamaschi, B.A., Fram, M.S., Fujii, R., Mopper, K., 2003. Evaluation of specific ultraviolet absorbance as an indicator of the chemical composition and reactivity of dissolved organic carbon. Environmental Science & Technology 37, 4702-4708.

Wilson, M.J., 1987. A Handbook of Determinative Methods in Clay Mineralogy. Chapman and Hall, New York.

Yong, R.N., Ohtsubo, M., 1987. Interparticle action and rheology of kaolinite-amorphous iron hydroxide (ferrihydrite) complexes. Applied Clay Science 2, 63-81.

Table 1. Physical and chemical properties of vermiculite (VM) and Fe (hydr)oxide-vermiculite (*x*Fe-VM) mixed systems.

Mineral	Fe_O (mol kg^{-1})	Fe_{DCB} (mol kg^{-1})	Fe_O/Fe_{DCB}	Fh[a] (g kg^{-1})	SSA (m^2 g^{-1})	Mesopore (2-50 nm) surface area (m^2 g^{-1})	Micropore (<2 nm) surface area (m^2 g^{-1})	ζ (mV)	σ_0 ($\mu mol_{(-)}$ m^{-2})
VM	nd	nd	–	nd	20.1	10.2	9.9	–39	15
1Fe-VM	1.07	1.31	0.82	103	23.3	12.8	10.6	–23	13
2Fe-VM	2.35	2.79	0.84	226	32.2	16.3	15.9	–10	8
3Fe-VM	3.98	4.68	0.85	383	39.4	18.9	20.5	–5.5	6
4Fe-VM	4.27	5.60	0.76	411	38.9	15.7	23.2	+8.0	5

[a] Ferrihydrite content estimated on the basis of Fe_O content.

Table 2. Chemical properties of the paddy soil-derived dissolved organic matter (*r*DOM) used for the sorption experiments.

C (g kg^{-1})	N (g kg^{-1})	C/N	COOH acidity (mmol mol^{-1} C)	Phenolic acidity (mmol mol^{-1} C)	C distribution (%)[a]				
					Alkyl C	Methoxy/ amine C	O-Alkyl C	Aromatic C	Carboxyl/ carbonyl C
442	45	9.8	104	109	26	11	24	26	13

[a] Percentage distribution of C determined from the integrals of ^{13}C-NMR regions relative to alkyl (0-40 ppm), methoxy/amine (40-60 ppm), O-alkyl (60-105 ppm), aromatic (105-165 ppm) and carboxyl/carbonyl (165-220 ppm) C.

Table 3. Langmuir and sigmoidal coefficients (± standard error) for the sorption of DOC on vermiculite (VM) and Fe (hydr)oxide-vermiculite mixed systems (*x*Fe-VM).

Mineral	Langmuir				Sigmoidal		
	K_L (l g^{-1})	Q_{max} (mg C g^{-1})	Q_{max} (mg C m^{-2})	R^2	Q_{max} (mg C g^{-1})	Q_{max} (mg C m^{-2})	R^2
VM	nd	nd	nd	nd	9.7 ± 0.7	0.49 ± 0.04	0.95
1Fe-VM	13 ± 6	25 ± 5	1.1 ± 0.2	0.87	18 ± 2	0.75 ± 0.07	0.89
2Fe-VM	7 ± 2	67 ± 11	1.9 ± 0.3	0.98	nd	nd	nd
3Fe-VM	67 ± 11	29 ± 1	0.74 ± 0.03	0.97	nd	nd	nd
4Fe-VM	41 ± 14	25 ± 2	0.65 ± 0.06	0.88	nd	nd	nd

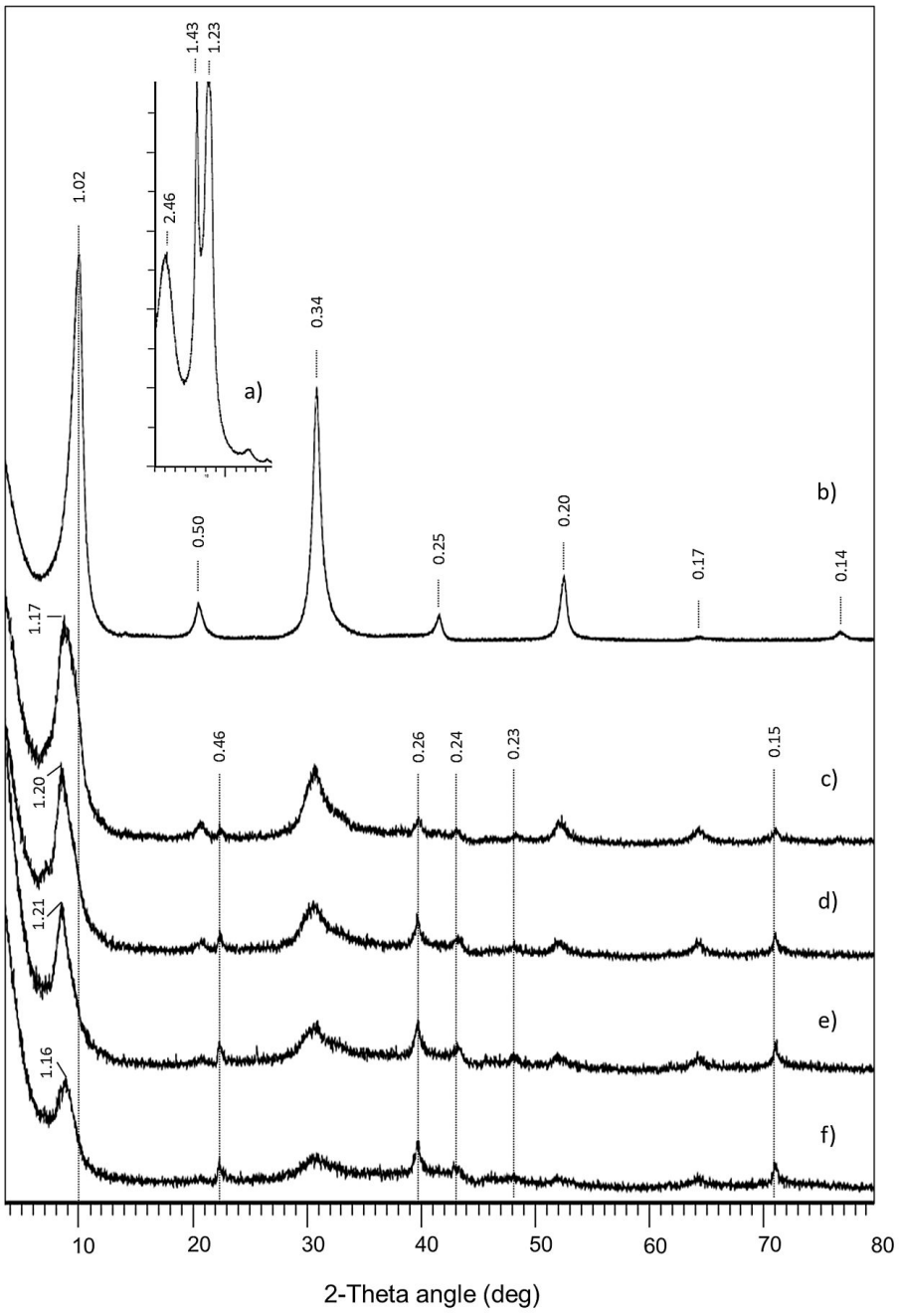

Figure 1: X-ray diffractograms of (a) Mg-saturated, and (b) K-saturated VM, as well as the synthesized Fe (hydr)oxide-vermiculite mixed systems (c) 1Fe-VM, (d) 2Fe-VM, (e) 3Fe-VM and (f) 4Fe-VM. Labels represent *d*-spacing values in nm. The patterns (a) and (b) have been scaled down by a factor of 0.2.

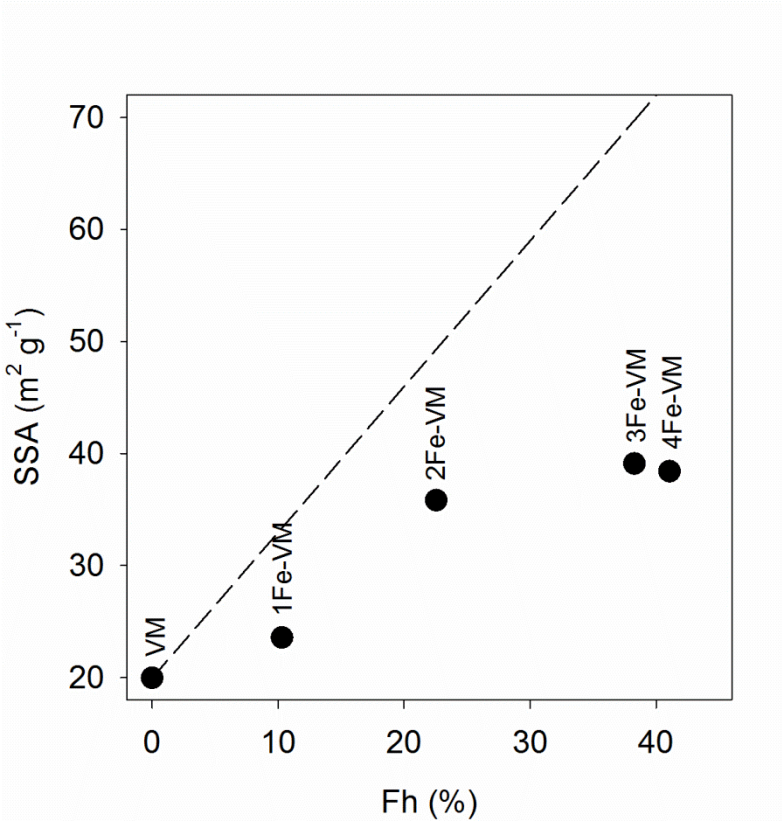

Figure 2: Variations in measured specific surface area (SSA) of the different minerals as a function of ferrihydrite (Fh) content. The dashed line represents theoretical values calculated as the additive combination of the surface areas of ferrihydrite and vermiculite.

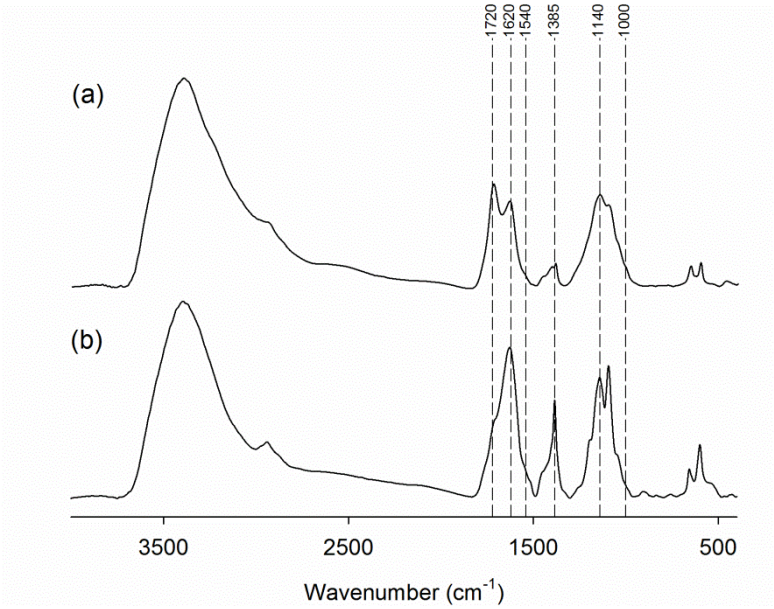

Figure 3: Fourier transform infrared spectra of *r*DOM at (a) pH 2.0, and (b) pH 5.5.

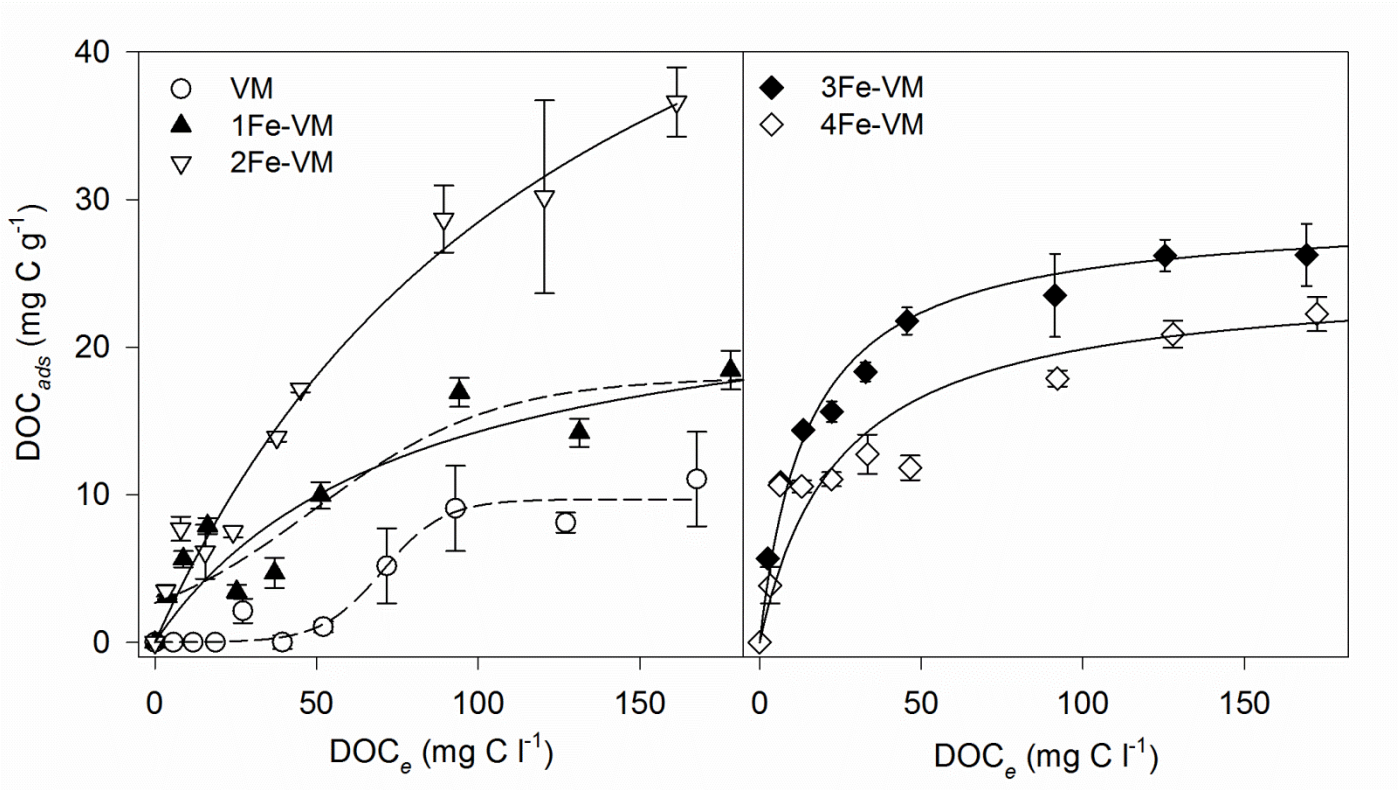

Figure 4: Sorption isotherms of DOC on vermiculite (VM) and Fe (hydr)oxide-vermiculite systems (*x*Fe-VM) at pH 5.5. Experimental data (symbols) were modelled with the Langmuir (complete line) and sigmoidal (dashed lines) equations. Error bars represent the standard error of the mean.

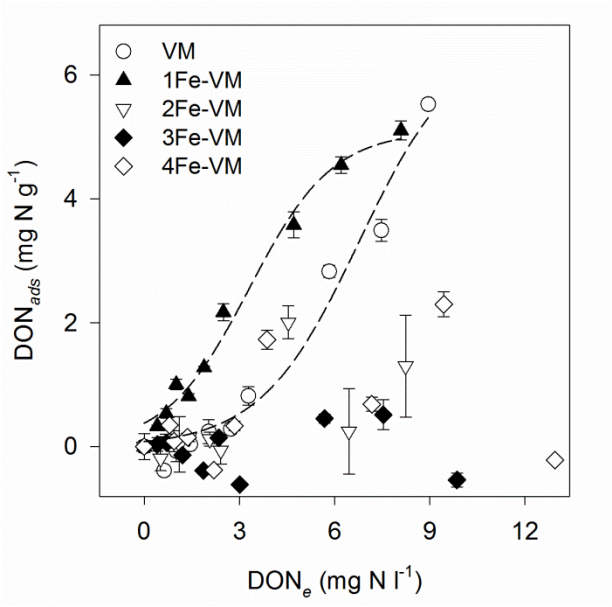

Figure 5: Sorption isotherms of DON on vermiculite (VM) and Fe (hydr)oxide-vermiculite systems (*x*Fe-VM) at pH 5.5. Experimental data (symbols) obtained for VM and 1Fe-VM were modelled with the sigmoidal equation (dashed lines). Error bars represent the standard error of the mean.

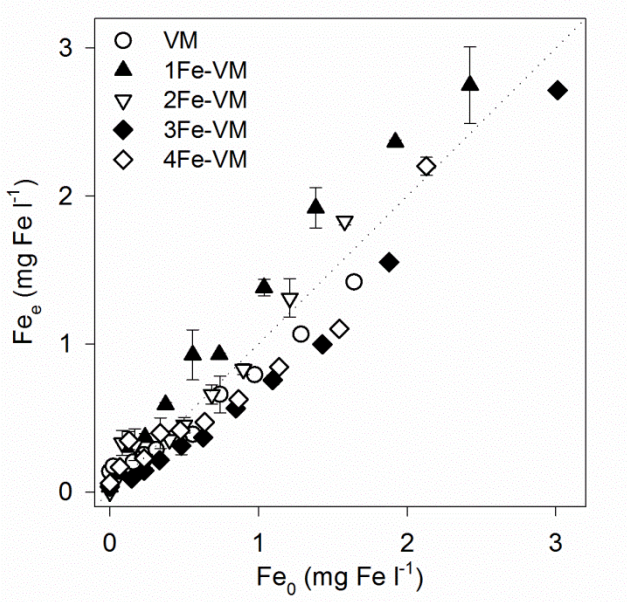

Figure 6: Comparison between equilibrium (Fe_e) and initial (Fe_0) concentrations of soluble Fe added with the *r*DOM as a function of DOC sorption on vermiculite (VM) and Fe (hydr)oxide-vermiculite systems (*x*Fe-VM) at pH 5.5. Dotted line represents the 1:1 relationship (i.e. no change). Error bars represent the standard error of the mean.

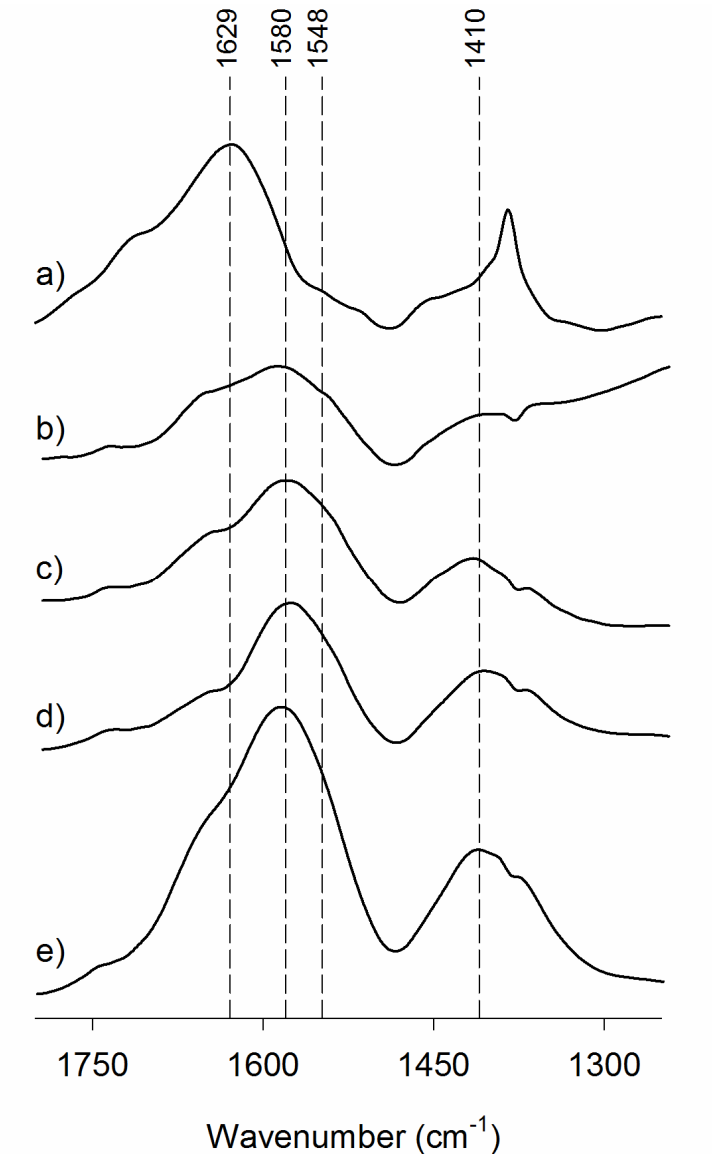

Figure 7: Fourier transform infrared spectra of *r*DOM (a) before sorption, and difference spectra of *r*DOM sorbed on Fe (hydr)oxide-vermiculite mixed systems (b) 1Fe-VM, (c) 2Fe-VM, (d) 3Fe-VM and (e) 4Fe-VM.

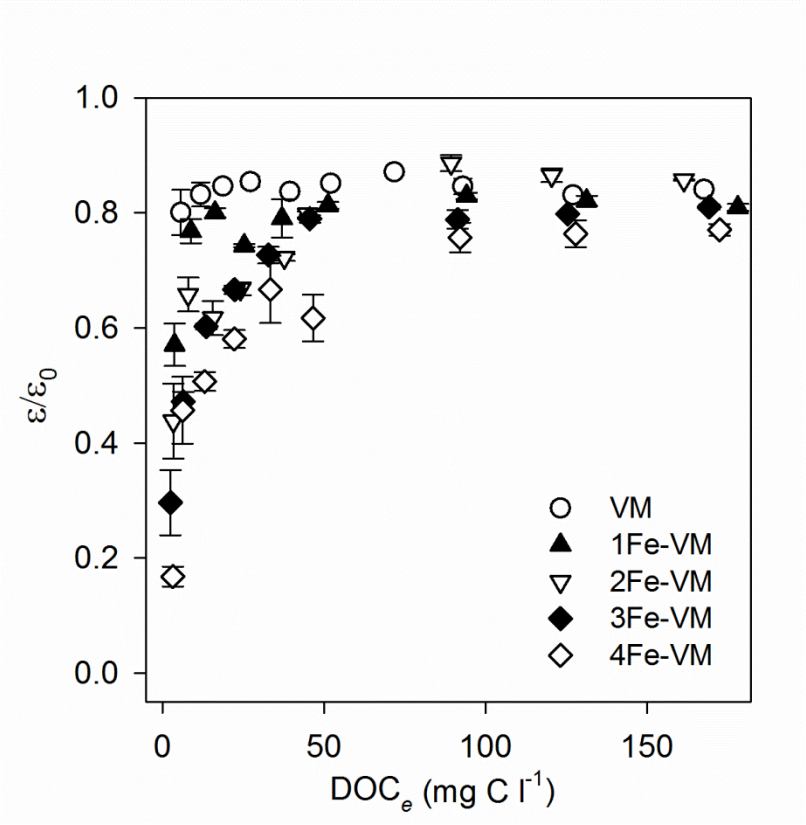

Figure 8: Variations in the molar UV absorbance (at 254 nm) of *r*DOM remaining at equilibrium (ε), relative to the molar UV absorbance of the initial *r*DOM solution (ε_0) as a function of DOC sorption on vermiculite (VM) and Fe (hydr)oxide-vermiculite systems (*x*Fe-VM) at pH 5.5. Error bars represent the standard error of the mean.

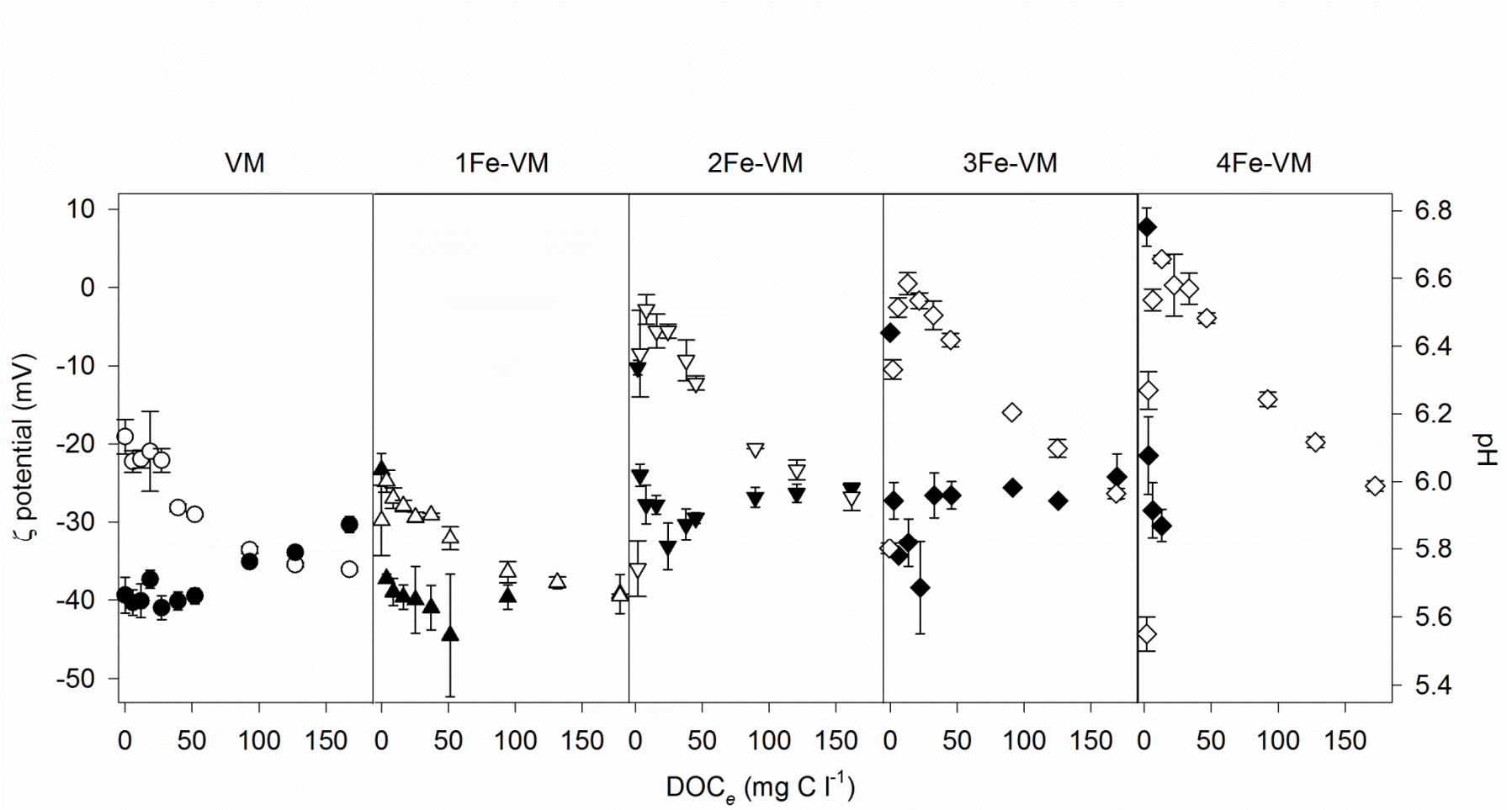

Figure 9: Variations in the solution pH at equilibrium (open symbols) and ζ potential of the suspensions (closed symbols) as a function of DOC sorption on vermiculite (VM) and Fe (hydr)oxide-vermiculite systems (*x*Fe-VM) at pH 5.5. Error bars represent the standard error of the mean.